Journal of Applied Physics ARTICLE scitation.org/journal/jap

Effects of surface recombination on the charge collection in h-BN neutron detectors

Cite as: J. Appl. Phys. **125**, 104501 (2019); doi: 10.1063/1.5089138
Submitted: 16 January 2019 · Accepted: 12 February 2019 ·
Published Online: 12 March 2019

A. Maity, S. J. Grenadier, J. Li, J. Y. Lin, and H. X. Jiang[a)]

AFFILIATIONS

Department of Electrical and Computer Engineering, Texas Tech University, Lubbock, Texas 79409, USA

[a)]Email: hx.jiang@ttu.edu

ABSTRACT

Hexagonal boron nitride (h-BN) epilayers have been recognized as a promising material for applications in solid-state neutron detectors. However, the highest detection efficiency of 58% attained so far for 1 mm^2 detectors fabricated from 50 μm thick B-10 enriched h-BN films still falls short of the expected theoretical value of 64%. This is due to the less than perfect charge collection efficiency. In this work, we have fabricated and analyzed the photocurrent-voltage characteristics of 11 h-BN neutron detectors. The dependence of the charge collection efficiency (η_c) on the charge carrier mobility-lifetime ($\mu\tau$) product of the bulk trapping parameter reveals that η_c is nearly perfect at a bias voltage of 200 V if we neglect the effects of surface recombination. Our results have clearly demonstrated that the surface recombination of charge carriers is the dominant factor that prevents a further enhancement in the charge collection efficiency in our current detectors. The surface recombination field E_S (=s/μ), defined as the ratio of the surface recombination velocity (s) to the carrier mobility (μ) of holes, was found to have a linear relationship with that of electrons and has a magnitude of the order of 10^4 V/cm. The present study indicates that it is critical to reduce E_S in h-BN in order to further push the charge collection and hence the total detection efficiency of h-BN neutron detectors to 100%.

INTRODUCTION

Neutron detectors are indispensable for the detection of fissile materials such as Plutonium-239 (^{239}Pu).[1] They are also needed in applications of geothermal and well-logging for the determination of porosity and water content of the rocks.[2] Pressurized Helium-3 ($^3He_2$) tubes are the most developed and widely deployed technology due to which He-3 has a high thermal neutron capture cross section of ~5330 b.[3] However, being gas-filled detectors, He-3 detectors have low atomic densities corresponding to long absorption lengths for thermal neutrons, making these detectors inherently bulky. Other disadvantages of He-3 detectors include the need for high pressurization and high voltage operation (>1000 V), slow response speed (~ms), low Q value (~0.764 MeV), and high ionization energy of gas. Moreover, the price of He-3 gas has increased dramatically in recent years. Therefore, extensive efforts have been devoted to the development of solid-state neutron detectors.[4–9] Hexagonal boron nitride (h-BN) has emerged as an important wide bandgap (6.0–6.4 eV) semiconductor for its applications in deep ultraviolet photonics[10–15] and solid-state neutron detectors.[16–23] Recent development of epitaxial growth processes for producing thick (~50 μm) B-10 enriched h-BN (h-^{10}BN) films using metal organic chemical vapor deposition (MOCVD) has led to the attainment of thermal neutron detectors with a 58% detection efficiency, which is the highest among all solid-state detectors.[23] This opens up the possibility of realizing solid-state neutron detectors which offer comparable performances but with more flexibilities in design as well as in form factors and lower manufacturing and maintenance costs compared with He-3 detectors.

The isotope B-10 has a large thermal neutron capture cross section of $\sigma \sim 3840$ b (=3.84×10^{-21} cm^2), whereas the density of B-10 atoms in h-^{10}BN is N [^{10}B] = 5.5×10^{22} cm^{-3}, which is about 550 times higher than that in He-3 gas pressurized at 4 atm. These together afford a relatively large absorption coefficient ($\Sigma = N\sigma = 5.5 \times 10^{22}$ $cm^{-3} \times 3.84 \times 10^{-21}$ $cm^2 = 211$ cm^{-1}) and a short absorption length ($\lambda = 1/\Sigma = 47.3$ μm) for thermal neutrons. The theoretical detection efficiency (η) of neutron detectors based on h-^{10}BN as a function of the detector's thickness, L, can be expressed in terms of the interaction probability as

$$\eta = P(L) = 1 - e^{-L/\lambda}, \quad (1)$$

where $\lambda = 47.3$ μm.[20,21] As such, an h-^{10}BN detector with a layer

thickness of $L = 3\lambda$ (~140 μm) can attain an intrinsic detection efficiency of 95%, and with a layer thickness of $L = 5\lambda$ (~250) μm, it can attain an intrinsic detection efficiency approaching 100%. However, the total detection efficiency also depends on the charge collection (or charge extraction) efficiency,[9] which is highly correlated with the material quality and carrier transport properties.

The capture of a thermal neutron (~25 meV) by a ^{10}B atom initiates the following nuclear reaction inside h-^{10}BN detectors:[3]

$$^{10}_{5}\mathrm{B} + {}^{1}_{0}\mathrm{n} = {}^{7}_{3}\mathrm{Li}^{*}\ (0.84\ \mathrm{MeV}) + {}^{4}_{2}\alpha^{*}\ (1.47\ \mathrm{MeV})\ [94\%\ \text{excited state}], \quad (2a)$$

$$^{10}_{5}\mathrm{B} + {}^{1}_{0}\mathrm{n} = {}^{7}_{3}\mathrm{Li}\ (1.015\ \mathrm{MeV}) + {}^{4}_{2}\alpha\ (1.777\ \mathrm{MeV})\ [6\%\ \text{ground state}], \quad (2b)$$

$$\mathrm{Li},\ \alpha \rightarrow N\ (\mathrm{e}^{-}) + \mathrm{N}\ (\mathrm{h}^{+}), \quad N \sim 10^{5}. \quad (3)$$

The high energy daughter particles ($^{7}_{3}$Li, $^{4}_{2}\alpha$) generated by the nuclear reaction of Eq. (2) decelerate through an h-^{10}BN detector material by depositing their energies, which create a cloud of electrons and holes inside h-^{10}BN, as described in Eq. (3). With the aid of an external applied electric field (E_a), these electrons and holes move across the detector toward anode and cathode and are then collected by the electrodes to serve as a detection signal of absorbed thermal neutrons.

It is well known from prior works on radiation detectors that the mobility-lifetime ($\mu\tau$) product which characterizes the process of bulk trapping is a key parameter that determines the detector performance.[24,25] This is because to the first order the condition for collecting the radiation-generated charge carriers is that the charge carrier drift length ($=\mu\tau E_a$) must be larger than the carrier transit distance (or the distance between the two electrodes, L), i.e., $\mu\tau E_a > L$, or $\mu\tau > L^2/V$ or $\frac{L^2}{V\mu\tau} < 1$, where V ($=E_a \cdot \mathrm{L}$) is the external voltage applied to the two electrodes. The relationship between $\mu\tau$ and V reveals that a material with a higher $\mu\tau$ product requires a lower applied bias voltage for sweeping out charge carriers, whereas the $\mu\tau$ product is correlated with the bulk material properties of the detector, including crystalline quality as well as the density of charge carrier traps.

Since the development of BN neutron detectors is in its early stage, all previous works conducted on BN neutron detectors have been primarily concentrated on increasing the film thickness to provide a reasonable intrinsic detection efficiency as well as on improving the $\mu\tau$ products with the aim of enhancing the charge collection efficiency at a reasonable bias voltage. For instance, the $\mu\tau$ products of our h-BN films have been improved from ~10^{-8} cm^2/V to >10^{-5} cm^2/V, whereas the film thickness has been increased from less than 1 μm to 50 μm over the last several years.[17,23] Subsequently, a detection efficiency of 58% has been achieved for 50 μm thick vertical detectors biased at 200 V.[23] However, the highest efficiency of 58% attained so far for 1 mm^2 detectors fabricated from 50 μm thick films is still lower than the theoretical efficiency of 64%, as expected from Eq. (1). This discrepancy is attributed to the less than perfect charge collection efficiency. In this work, we aim to investigate the mechanisms that limit the charge collection efficiency. By evaluating a set of 11 detectors, we demonstrate that the surface effects (charge carrier trapping and recombination at surfaces) are a key factor that prevents a further increase in the charge collection and hence limits the total detection efficiency of h-^{10}BN neutron detectors.

EXPERIMENTS

^{10}B enriched h-BN epilayers were grown using MOCVD on *c*-plane sapphires of 4-in. in diameter. Precursors for the chemical reaction were 99.9% ^{10}B-enriched trimethylboron and ammonia (NH_3), and H_2 was used as a carrier gas.[21–23,26] One of the unique properties of h-BN epilayers is the ability of obtaining freestanding wafers without invoking techniques such as the laser lift-off as for other III-nitrides. Due to the difference in thermal expansion coefficients between h-BN and sapphire substrate and the layer structure nature of h-BN, thick h-^{10}BN epilayers with a sufficient thickness (>30 μm) naturally separate from the sapphire substrate during cooling down after growth, providing freestanding h-^{10}BN wafers as schematically depicted in Fig. 1(a). An image of a freestanding h-^{10}BN wafer of 4-in. in diameter is shown in Fig. 1(b). The electron-beam evaporation technique was used to deposit Ohmic contacts consisting of the Ni (10 nm)/Au (20 nm) bilayer on both sides of the freestanding h-^{10}BN to form a vertical photoconductive type of detectors, as schematically represented in Fig. 1(c). Detectors consisting of the Ti (10 nm)/Al (20 nm) bilayer were also fabricated for the purpose of conducting comparison studies on the effects of different metal contacts on the surface recombination. The use of these metals as Ohmic contacts was adopted from GaN devices. Figure 1(d) shows a dark current-voltage (I-V) characteristic of a 50 μm thick vertical detector with a detection area of 1 mm^2 incorporating Ni (10 nm)/Au (20 nm) bilayer as electrodes, revealing an Ohmic behavior. As shown in Fig. 1(d), the typically leakage current densities of h-^{10}BN detectors are very low, around 1×10^{-10} A/cm^2 at a bias voltage of 200 V (or at an applied electric field of 4×10^4 V/cm) due to the large bandgap of h-BN, rendering these materials highly resistive. In contrast to conventional III-nitride wide bandgap semiconductors, the as-deposited metal contacts on h-BN exhibit Ohmic behavior without additional thermal annealing.

The mobility-lifetime ($\mu\tau$) products and the surface recombination velocities for electrons and holes were obtained by measuring the photocurrent-voltage (I-V) characteristics with either the anode or the cathode of the detector surface irradiated with a UV light (a deuterium UV lamp consisting of a continuum spectrum from 190 to 350 nm) and analyzed using the classical Many's equation.[24]

RESULTS AND DISCUSSION

In h-BN, above bandgap photons have a very high optical absorption coefficient (~7×10^5/cm), corresponding to a short optical absorption length (λ) of 14.5 nm.[15,27] Therefore, the penetration depth of the above bandgap photons is within ~70 nm (5λ) from the irradiated surface, which is much smaller than the thickness (~50 μm) of the detectors. As such, the applied voltage polarity can be set up as to either inject electrons or holes from the illuminated surface into the bulk, as depicted in Fig. 1(c), so that the transport properties of electrons and holes can be separately

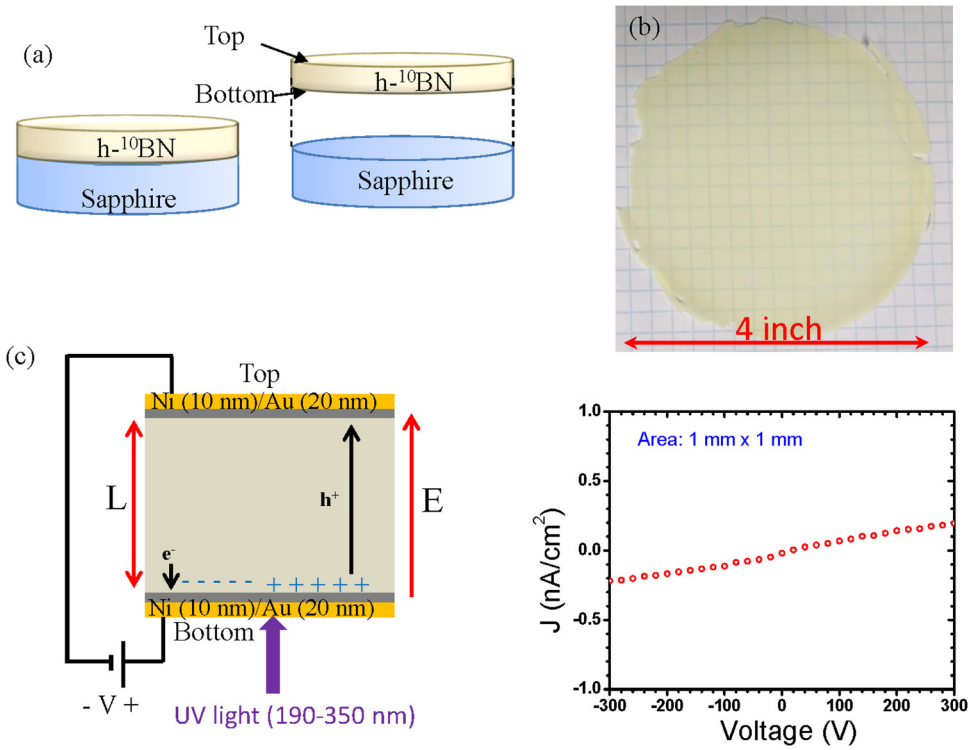

FIG. 1. (a) Schematic diagram of a freestanding h-^{10}BN wafer formed by self-separation from the sapphire substrate during cooling down after MOCVD growth. (b) Photo of a freestanding h-^{10}BN epilayer wafer of 4-in. in diameter. (c) Schematic diagram of a h-^{10}BN vertical detector with its anode bottom surface irradiated with UV radiation, allowing the probe of the hole transport properties in the detector material. (d) Dark (leakage) current vs applied voltage (or I-V characteristic) of a 1 mm^2 neutron detector fabricated from a 50 μm thick h-^{10}BN epilayer.

probed. The photocurrent as a function of the applied voltage under UV excitation for a set of 11 detectors of 1 mm^2 in size was measured and analyzed based on the classical Many's equation for insulating semiconductors under strongly absorbed illumination by taking into consideration of both effects of surface recombination and bulk trapping[24]

$$I_i(V) = I_{0,i}\,[\eta_{c,i}(V)],$$
$$= I_{0,i}\left[\frac{V\mu_i\tau_i\left(1-e^{-\frac{L^2}{V\mu_i\tau_i}}\right)}{L^2\left(1+\frac{s_iL}{\mu_iV}\right)}\right], \quad (i=e,\ h), \tag{4}$$

where $\eta_c(V)$ defines as the charge collection efficiency at an external bias voltage (V) applied between the two electrodes, I_0 is the saturation current, $\mu_h\tau_h$ ($\mu_e\tau_e$) and s_h (s_e) denote, respectively, the mobility-lifetime product and surface recombination velocity for holes (electrons), and L is the thickness of the detector (or the carrier transit length). For the purpose of illustration, I-V characteristic for the hole transport under UV excitation for a representative 50 μm thick detector is shown in Fig. 2. Fitting with Eq. (4) yields values of $\mu_h\tau_h$ and s_h/μ_h of 1.0×10^{-4} cm^2/V and 9.6×10^3 V/cm, respectively.

By examining Eq. (4), one can see that other than the condition of $\mu\tau E_a > L$ or $\frac{L^2}{V\mu\tau} < 1$ appeared in the numerator, another condition for attaining a high charge collection efficiency contained in the denominator is $\frac{sL}{\mu V} < 1$, which is governed by the surface recombination velocities. By defining s/μ as the "surface recombination field," E_S, we can rewrite this condition as $\frac{s/\mu}{V/L} = \frac{E_S}{E_a} < 1$, where E_a $\left(=\frac{V}{L}\right)$ is the external applied electric field. Introducing E_S is useful for understanding the effects of surface recombination on the charge collection efficiency. Not only the ratio of the surface recombination velocity to mobility is a measure of an "effective electric field" at the surfaces, but also it provides a direct way for quantifying the necessary charge collection condition with respect to the applied electric field, that is, $\frac{E_S}{E_a} < 1$. In other words, other than the charge transport processes occurring in the bulk as described in the numerator of Eq. (4), photo- or neutron-generated charge carriers must also overcome the surface trap induced potential barriers or surface recombination fields at both surfaces in order to be extracted by the electrodes. This scenario is schematically illustrated in Fig. 3. As such, the external applied electric field must be much greater than the surface recombination field, $E_a \gg E_S$, in order to effectively sweep out charge carriers.

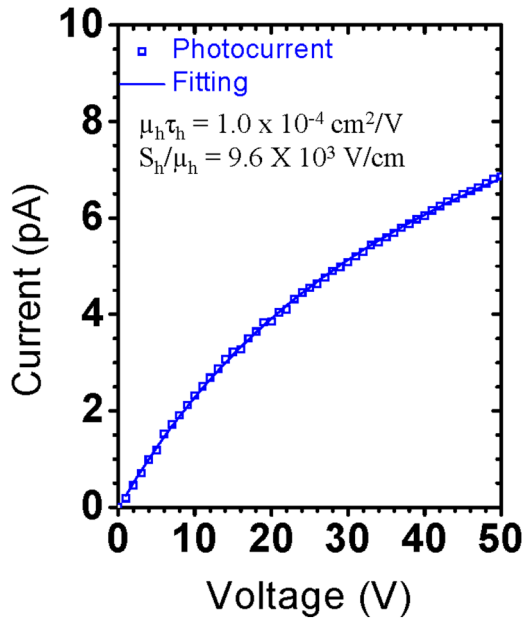

FIG. 2. Photocurrent-voltage characteristic for the hole transport of a 50 μm thick vertical h-^{10}BN detector measured under UV excitation. Measured $\mu\tau$ product and surface recombination field s/μ are indicated.

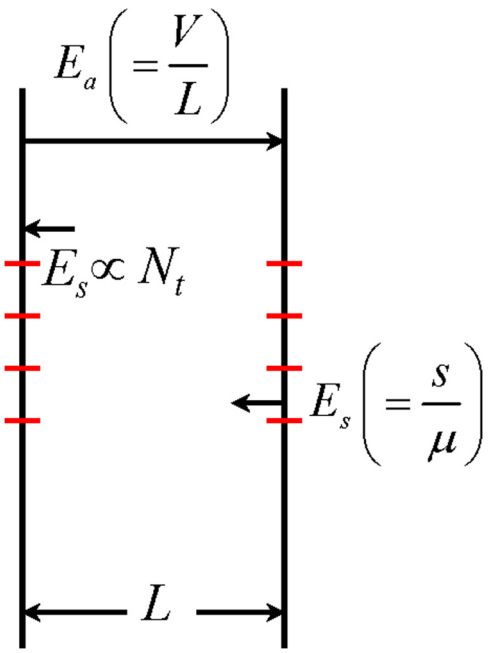

FIG. 3. Schematic representation of relation between "surface recombination field" (E_s) and surface trap density (N_t). The direction of E_S (=s/μ) is opposite to the applied electric field E_a (=V/L).

Surface trap states are formed due to the presence of impurities at both surfaces, which act as recombination centers for neutron- or photo-generated charge carriers in addition to bulk traps. To the first order, the surface recombination rate can be written as $R_s \propto s \propto \sigma_t N_t$, where σ_t and N_t denote the recombination cross section and density of the surface traps, respectively. Hence, the surface field, $E_s = s/\mu$, is also proportional to the surface trap density and inversely proportional to the carrier mobility, whereas its direction is always opposite to the applied electric field, E_a, as indicated in Fig. 3.

To investigate the dominant factors which are limiting the charge collection efficiency, following Eq. (4), we plot in Fig. 4 the calculated values of (a) $\frac{L^2}{V\mu\tau}$ and (b) $\frac{sL}{\mu V}$ as functions of the applied voltage (V) up to 200 V for several different values of $\mu\tau$ products between 10^{-6} and 10^{-4} cm^2/V and s/μ between 10^2 and 10^5 V/cm. To achieve a high charge collection efficiency (η_c), it is preferable that both conditions of $\frac{L^2}{V\mu\tau} \ll 1$ and $\frac{sL}{\mu V} \ll 1$ are satisfied. Plots shown in Fig. 4(a) are predominantly determined by the bulk trapping as represented by the numerator of Eq. (4), which provide a useful guidance on the attainable η_c at a certain bias voltage for a given material (with a fixed $\mu\tau$ product value). Plots shown in Fig. 4(b) are dominated by the surface effects contained in the denominator of Eq. (4)

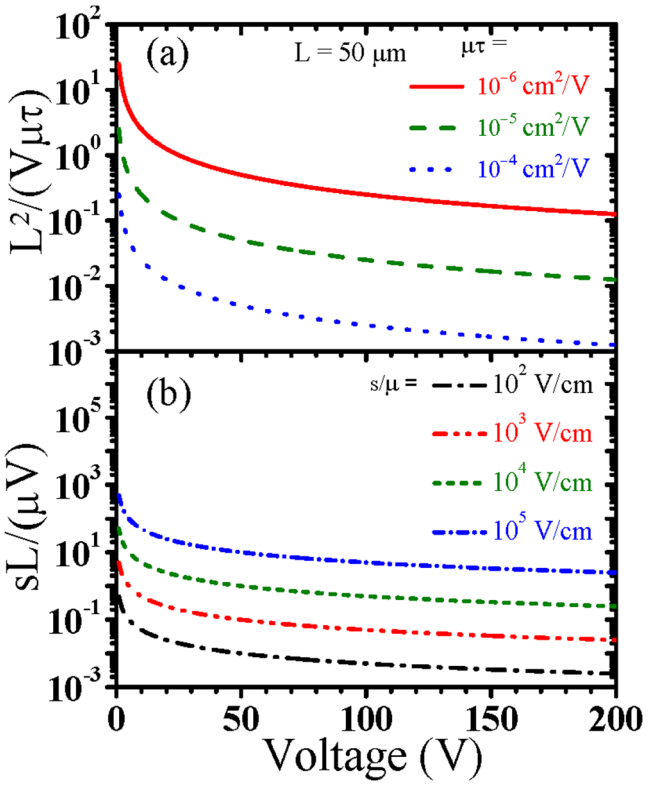

FIG. 4. Plot of bias voltage V dependence of (a) $\frac{L^2}{V\mu\tau}$ for $\mu\tau$ products of 10^{-6}, 10^{-5}, and 10^{-4} cm^2/V; (b) plot of bias voltage V dependence of $\frac{sL}{\mu V}$ for s/μ values of 10^2, 10^3, 10^4, and 10^5 V/cm for 50 μm thick h-BN detectors.

and represent achievable η_c at a certain bias voltage at a given surface condition (or a surface recombination field).

As most of our thick h-BN samples possess $\mu\tau$ products of about 10^{-5} cm^2/V or greater, the condition for overcoming the bulk trapping of $\frac{L^2}{V\mu\tau} \ll 1$ ($<10^{-2}$ or below) is already satisfied at a bias voltage of 200 V, as shown in Fig. 4(a). This implies that further improvement in the $\mu\tau$ products will not increase significantly the charge collection efficiency as the values of the numerator $\frac{V\mu_i\tau_i}{L^2}(1-e^{-\frac{L^2}{V\mu_i\tau_i}})$ in Eq. (4) for most of our detectors are already approach >99%. The high values of this term helped to bring down the required bias voltage for retaining relatively high efficiencies for our detectors. However, the measured values of E_S ($=s/\mu$) of our thick h-BN samples are between 10^3 and10^4 V/cm, providing values of $\frac{E_s^i}{E_a}(=\frac{s_iL}{\mu_iV}) < 25\%$ at a bias voltage of 200 V, as depicted in Fig. 4(b). The results thus indicate that presently the charge collection efficiency of our h-BN neutron detectors is limited by the surface recombination.

This point is further illuminated in Fig. 5, where the values of the numerator of Eq. (4), $\frac{V\mu_i\tau_i}{L^2}(1-e^{-\frac{L^2}{V\mu_i\tau_i}})$, are plotted against those of the denominator of Eq. (4), $\frac{1}{(1+\frac{s_iL}{\mu_iV})}$ or $\frac{1}{(1+\frac{E_s^i}{E_a})}$, using the measured $\mu\tau$ product and s/μ values obtained from a set of 11 h-BN neutron detectors fabricated from various samples. Ideally, both terms need to approach 100% in order to achieve a perfect charge collection efficiency. The majority of detectors have $\mu\tau$ product values of $\sim 10^{-5}$ cm^2/V or greater and are clustered together where values of $\frac{V\mu_i\tau_i}{L^2}(1-e^{-\frac{L^2}{V\mu_i\tau_i}})$ are mostly greater than 99%. This means that the charge collection efficiency approaches >99% if we consider the bulk transport alone. However, the values of the surface related term, $1/(1+\frac{s_iL}{\mu_iV})$, have a much larger variation, ranging from 70% to 90%. For instance, the measured $\mu_h\tau_h$ and $\mu_e\tau_e$ products for device #7 with a thickness of 35 μm are 1.5×10^{-5} and 0.7×10^{-5} cm^2/V, which provide values of 99.8% and 99.6% at a bias voltage of 200 V for $\frac{V\mu_i\tau_i}{L^2}(1-e^{-\frac{L^2}{V\mu_i\tau_i}})$ for holes and electrons, respectively. However, the measured "surface recombination fields" for the same device are 2.1×10^4 and 1.8×10^4 V/cm for holes and electrons, respectively, giving values of 72.7% and 76.5% at a bias voltage of 200 V for $1/(1+\frac{s_iL}{\mu_iV})$ for holes and electrons, respectively. These lead to overall charge collection efficiencies for holes and electrons in device #7 of 72.6% and 76.1%, respectively. Therefore, the results again confirm that the overall charge collection efficiencies are largely limited by the surface recombination fields. Consequently, minimizing the surface recombination velocities or equivalently minimizing the ratio of E_S/E_a is necessary to further improve the charge collection efficiency. On the other hand, increasing the applied voltage (or E_a) can help to thrust the charge carriers to overcome the surface recombination fields and push the term of $1/(1+\frac{s_iL}{\mu_iV})$ close to 100% but is less practical for applications.

In Fig. 6, the "surface recombination fields" for holes are plotted against those of electrons for the same set of 11 h-BN

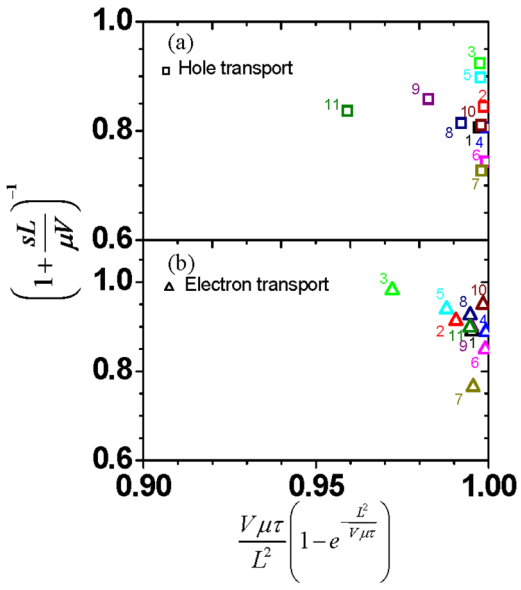

FIG. 5. Plot of the numerator $\frac{V\mu\tau}{L^2}(1-e^{-\frac{L^2}{V\mu\tau}})$ in Eq. (4) vs. the denominator $1/(1+\frac{sL}{\mu V})$ in Eq. (4) for photo-excited (a) hole and (b) electron transport, using the measured $\mu\tau$ product and s/μ values obtained from a set of 11 h-BN neutron detectors with a detection area of 1 mm × 1 mm fabricated from different samples.

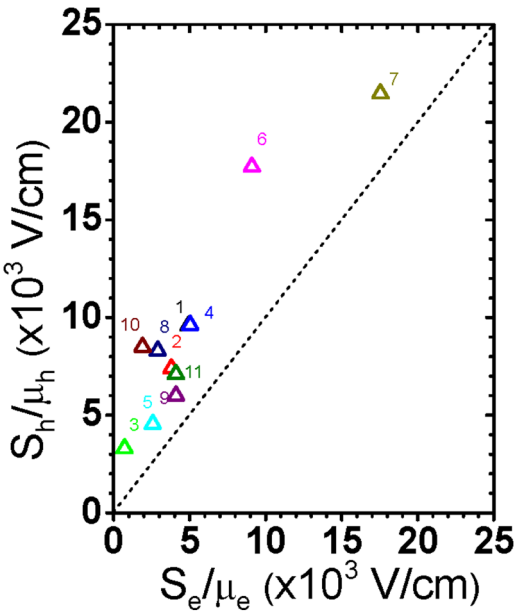

FIG. 6. Plot of the "surface recombination field" for hole (s_h/μ_h) vs electron (s_e/μ_e) for a set of 11 h-BN detectors of 1 mm × 1 mm in detection area. The dotted line indicates $s_h/\mu_h = s_e/\mu_e$.

detectors. The dotted line represents the case $E_s^h = \frac{s_h}{\mu_h} = \frac{s_e}{\mu_e} = E_s^e$. It is apparent that values of E_S for holes are above this line, whereas those of electrons are below this line for the condition shown in Fig. 1(c) with the bottom surface being irradiated. This implies that E_s^h is larger than E_s^e. The results not only suggest that h-BN surfaces contain traps for both types of charge carries, but the surfaces contain more traps for holes than for electrons.

Figure 7 plots the "surface recombination fields," s/μ, for neutron detectors of two different sizes, 1 and 9 mm^2 fabricated from a 50 μm thick sample. The "surface recombination field" appears to increase with increasing detector size. It is well known in the radiation detector field that enlargement of detection area is a key to achieve highly sensitive neutron detectors. Therefore, reducing E_S is not only important for attaining neutron detectors with higher detection efficiencies but is also necessary for achieving detectors with higher sensitivities.

As Ni/Au and Ti/Al bilayers were widely used, respectively, as Ohmic contacts for p-type and n-type GaN devices, we have also examined Ti/Al bilayers as Ohmic contacts for h-BN detectors aimed at reducing the surface recombination effects. A recent calculation revealed that the Schottky barrier heights of Ni and Ti on p-type (n-type) h-BN were 2.2 eV (4.3 eV) and 2.34 eV (4.16 eV), respectively.[28] However, our undoped h-BN epilayers are highly insulating, which makes examination of Ti/Al bilayer as another possible Ohmic contact on h-BN a worthy study. Figure 8 compares the "surface recombination fields" of electrons between two 1 mm^2 neutron detectors fabricated from a 50 μm thick h-^{10}BN wafer using metal contacts of Ni/Au (10 nm/20 nm) and Ti/Al (10 nm/20 nm) bilayers. We found that Ni/Au bilayer produces a smaller E_S than that of Ti/Al bilayer. Hence, Ni/Au bilayer is

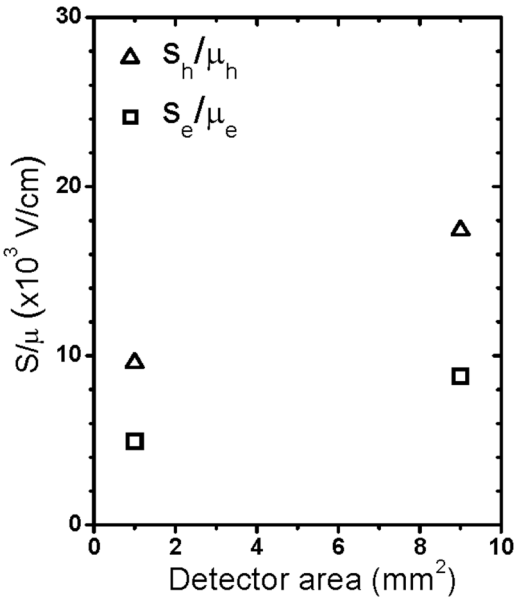

FIG. 7. Plot of the "surface recombination field" (s/μ) for two detectors with different detection areas (A) fabricated from a 50 μm thick h-^{10}BN sample.

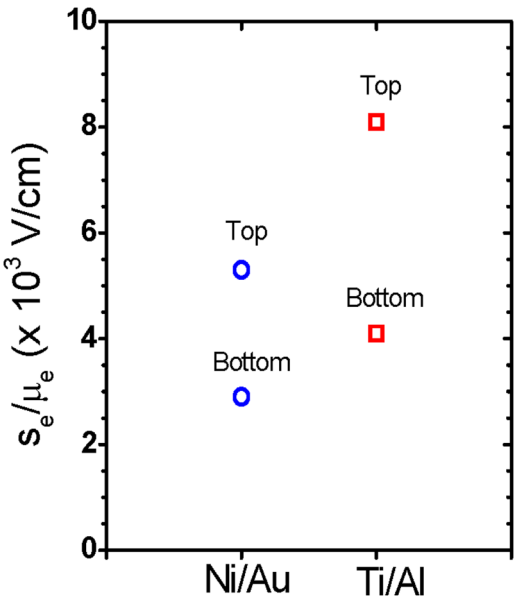

FIG. 8. Plot of the "surface recombination field" for electron transport (s_e/μ_e) for two detectors fabricated from a 50 μm thick h-^{10}BN sample using metal contacts of Ni/Au (10 nm/20 nm) and Ti/Al bilayers (10 nm/20 nm).

preferred over Ti/Al bilayer for the fabrication of h-^{10}BN detectors, which corroborates our previous measurement results on leakage currents and overall thermal neutron detection efficiencies.[23]

Surface traps on h-BN surfaces could form due to the presence of intrinsic defects such as nitrogen vacancy V_N (donor) and boron vacancy V_B (acceptor) or impurities like oxygen occupying nitrogen site O_N (donor) and carbon occupying nitrogen site C_N (acceptor).[26] There is also a possibility that impurities tend to attach to the surfaces of h-BN from air. Thus, apart from enhancing the material purity and crystalline quality through epitaxial growth, surface protection of h-BN films needs to be investigated along with the development of effective surface cleaning and surface treatment techniques.

In summary, considering the results from bulk trapping ($\mu\tau$) and surface recombination (s/μ), we have identified that the surface effects are the primary factor that prevents further improvement in the charge collection efficiency in our current vertical h-^{10}BN detectors. At the current stage of development, as most of our detectors exhibit charge collection efficiencies of greater than 99% at a bias voltage of 200 V by considering the bulk transport alone, bulk trapping appears to be a less serious issue. It is the surface recombination that limits the overall charge collection efficiency to below 90%. Experimental data also revealed that the surface recombination effects will hamper the development of large neuron detectors as the surface recombination field increases with the detector size. Our results also showed that the surfaces of our current h-BN samples contain more traps for holes than for electrons. We have also identified that the Ni/Au bilayer is more suitable than the Ti/Al bilayer as an Ohmic contact for h-^{10}BN neutron detectors as it yields a lower "surface recombination field."

The present studies strongly indicate that approaches for reducing the density of surface recombination centers must be explored, especially for the fabrication of large area detectors. These possibly include device processing optimization, appropriate surface treatments, and device passivation. Moreover, enhancing the carrier mobility (μ) will be very beneficial because this improves simultaneously the bulk and surface transport properties by increasing the $\mu\tau$ product and decreasing the surface recombination field (s/μ). However, improving the carrier mobility requires further advances in the MOCVD growth processes to improve the crystalline quality and purity as well as to reduce defects and impurities which all act as charge carrier traps.

Acknowledgments

This research was supported by DOE ARPA-E (No. DE-AR000964). DOE NSSA SSAA program (No. DE-NA0002927) supported the initial h-BN detector development efforts. H. X. Jiang and J. Y. Lin are grateful to the AT&T Foundation for the support of Ed Whitacre and Linda Whitacre endowed chairs.

REFERENCES

[1]W. A. Noonan, Johns Hopkins APL Technical Digest **32**, 762 (2014).
[2]J. Neal, L. Boatner, Z. Bell, H. Akkurt, and M. McCarthy, "Evaluation of neutron and gamma detectors for high-temperature well-logging applications," in *Future of Instrumentation International Workshop (FIIW)* (IEEE Xplore 2011), pp. 172–175.
[3]G. F. Knoll, *Radiation Detection and Measurement*, 4th ed. (John Wiley & Sons, 2010).
[4]F. P. Doty, "Boron nitride solid-state neutron detector," U.S. patent 6,727,504 (April 27, 2004).
[5]J. Uher, S. Pospisil, V. Linhart, and M. Schiebar, Appl. Phys. Lett. **90**, 124101 (2007).
[6]Q. Shao, L. F. Voss, A. M. Conway, R. J. Nikolic, M. A. Dar, and C. L. Cheung, Appl. Phys. Lett. **102**, 063505 (2013).
[7]S. L. Bellinger, R. G. Fronk, W. J. McNeil, T. J. Sobering, and D. S. McGregor, IEEE Trans. Nucl. Sci. **59**, 167 (2012).
[8]K. Osberg, N. Schemm, S. Balkir, J. O. Brand, M. S. Hallbeck, P. A. Dowben, and M. W. Hoffman, IEEE Sens. J. **6**, 1531 (2006).
[9]E. Echeverria, B. Dong, G. Peterson, J. P. Silva, E. R. Wilson, M. S. Driver, Y. S. Jun, G. D. Stucky, S. Knight, T. Hofmann, Z. K. Han, N. Shao, Y. Gao, W. N. Mei, M. Nastasi, P. A. Dowben, and J. A. Kelber, J. Phys. D Appl. Phys. **49**, 355302 (2016).
[10]K. Watanabe, T. Taniguchi, and H. Kanda, Nat. Mater. **3**, 404 (2004).
[11]Y. Kubota, K. Watanabe, O. Tsuda, and T. Taniguchi, Science **317**, 932 (2007).
[12]K. Watanabe, T. Taniguchi, T. Niiyama, K. Miya, and M. Taniguchi, Nat. Photonics **3**, 591 (2009).
[13]R. Dahal, J. Li, S. Majety, B. N. Pantha, X. K. Cao, J. Y. Lin, and H. X. Jiang, Appl. Phys. Lett. **98**, 211110 (2011).
[14]S. Majety, J. Li, X. K. Cao, R. Dahal, B. N. Pantha, J. Y. Lin, and H. X. Jiang, Appl. Phys. Lett. **100**, 061121 (2012).
[15]J. Li, S. Majety, R. Dahal, W. P. Zhao, J. Y. Lin, and H. X. Jiang, Appl. Phys. Lett. **101**, 171112 (2012).
[16]J. Li, R. Dahal, S. Majety, J. Y. Lin, and H. X. Jiang, Nucl. Instrum. Methods Phys. Res. A **654**, 417 (2011).
[17]T. C. Doan, S. Majety, S. Grenadier, J. Li, J. Y. Lin, and H. X. Jiang, Nucl. Instrum. Methods Phys. Res. A **748**, 84 (2014).
[18]T. C. Doan, S. Majety, S. Grenadier, J. Li, J. Y. Lin, and H. X. Jiang, Nucl. Instrum. Methods Phys. Res. A **783**, 121 (2015).
[19]T. C. Doan, J. Li, J. Y. Lin, and H. X. Jiang, AIP Adv. **6**, 075213 (2016).
[20]K. Ahmed, R. Dahal, A. Weltz, J. J.-Q. Lu, Y. Danon, and I. B. Bhat, Appl. Phys. Lett. **110**, 023503 (2017).
[21]A. Maity, T. C. Doan, J. Li, J. Y. Lin, and H. X. Jiang, Appl. Phys. Lett. **109**, 072101 (2016).
[22]A. Maity, S. J. Grenadier, J. Li, J. Y. Lin, and H. X. Jiang, Appl. Phys. Lett. **111**, 033507 (2017).
[23]A. Maity, S. J. Grenadier, J. Li, J. Y. Lin, and H. X. Jiang, J. Appl. Phys. **123**, 044501 (2018).
[24]A. Many, J. Phys. Chem. Solids **26**, 575 (1965).
[25]T. Takahashi and S. Watanabe, IEEE Trans. Nucl. Sci. **48**, 950 (2001).
[26]S. J. Grenadier, A. Maity, J. Li, J. Y. Lin, and H. X. Jiang, Appl. Phys. Lett. **112**, 162103 (2018).
[27]T. Sugino, K. Tanioka, S. Kawasaki, and J. Shirafuji, Jpn. J. Appl. Phys. Part 2 **36**, L463 (1997).
[28]M. Bokdam, G. Brocks, M. I. Katsnelson, and P. J. Kelly, Phys. Rev. B **90**, 085415 (2014).